

pubs.acs.org/NanoLett Letter

Van der Waals Superstructure and Twisting in Self-Intercalated Magnet with Near Room-Temperature Perpendicular Ferromagnetism

Amanda L. Coughlin, Dongyue Xie, Xun Zhan, Yue Yao, Liangzi Deng, Heshan Hewa-Walpitage, Trevor Bontke, Ching-Wu Chu, Yan Li, Jian Wang, Herbert A. Fertig, and Shixiong Zhang*



Cite This: Nano Lett. 2021, 21, 9517-9525



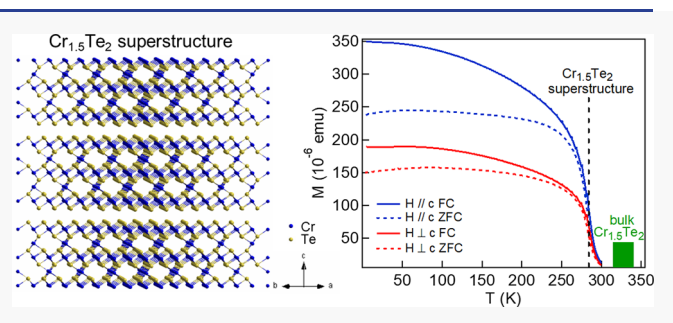
ACCESS

III Metrics & More

Article Recommendations

Supporting Information

ABSTRACT: The emergence of van der Waals (vdW) magnets has created unprecedented opportunities to manipulate magnetism for advanced spintronics based upon all-vdW heterostructures. Among various vdW magnets, $Cr_{1+\delta}Te_2$ possesses high temperature ferromagnetism along with possible topological spin textures. As this system can support self-intercalation in the vdW gap, it is crucial to precisely pinpoint the exact intercalation to understand the intrinsic magnetism of the system. Here, we developed an iterative method to determine the self-intercalated structures and show evidence of vdW "superstructures" in individual $Cr_{1+\delta}Te_2$ nanoplates exhibiting magnetic behaviors distinct from bulk



chromium tellurides. Among 26,332 possible configurations, we unambiguously identified the Cr-intercalated structure as 3-fold symmetry broken $Cr_{1.5}Te_2$ segmented by vdW gaps. Moreover, a twisted Cr-intercalated layered structure is observed. The spontaneous formation of twisted vdW "superstructures" not only provides insight into the diverse magnetic properties of intercalated vdW magnets but may also add complementary building blocks to vdW-based spintronics.

KEYWORDS: 2D magnets, van der Waals materials, chromium telluride, self-intercalation, twisting

Van der Waals (vdW) magnets (Cr₂Ge₂Te₆¹ and CrI₃²) have recently emerged as a fascinating magnetic material system to explore intrinsic magnetism and emergent phenomena in the two-dimensional (2D) limit.^{3–8} In comparison to the atomically thin magnetic films extensively studied in the 1980–90s,^{9,10} 2D vdW magnets are advantageous as they can be readily stacked into 2D heterostructures¹¹ and their magnetic properties can be sensitively tuned by external stimuli including electric field, ^{12–14} strain,¹⁵ electrostatic doping,¹⁶ and so forth. Indeed, the ability to finely stack, control, and engineer the magnetism of these 2D vdW materials layer by layer facilitates the development of novel magnetoelectric and spintronic devices, such as vertical field effect transistors, ^{17,18} tunneling-based memory, logic, and spinflltering devices.

While many efforts have been focused on studying transition metal trihalides (e.g., CrI_3), $^{2,16,23-30}$ they have often been shown to be unstable and degrade within minutes in air and/or when exposed to light, 31 requiring either *in situ* measurements in an oxygen-free environment or encapsulation between protective layers to prevent deterioration. 2,21 Conversely, transition metal telluride compounds are expected to be relatively more stable in ambient conditions. Among various vdW magnetic tellurides, the binary chromium telluride 1T- $CrTe_2$ has a ferromagnetic ordering temperature T_c above

room temperature, ^{32–36} which is significantly higher than that of the previously studied ternary chromium tellurides $Cr_2X_2Te_6$ (X=Si, Ge). ^{1,14,37–44} Furthermore, a colossal anomalous Hall conductivity was recently observed in 1T- $CrTe_2$ with simultaneously large anomalous Hall angles and electrical conductivities distinct from other anomalous Hall materials, making it an excellent candidate for spintronics applications. ^{33,45} By intercalating Cr atoms into the vdW gap between the $CrTe_2$ layers, as shown in Figure 1a, different chromium telluride compounds $Cr_{1+\delta}Te_2$ ($0 < \delta \le 1$) are created. These different $Cr_{1+\delta}Te_2$ phases have a broad range of magnetic ordering temperatures and novel magnetic phases. ^{32,34,35,46–56} For example, CrTe (or Cr_2Te_2) thin films have been reported to exhibit the topological Hall effect, noted as strong evidence of a magnetic skyrmion phase. ⁵⁷ Similar topological spin textures have also been reported in Cr_2Te_3 (or $Cr_{1,33}Te_2$) thin films embedded with bismuth nanosheets. ⁵⁸

Received: July 30, 2021
Revised: October 26, 2021
Published: November 3, 2021





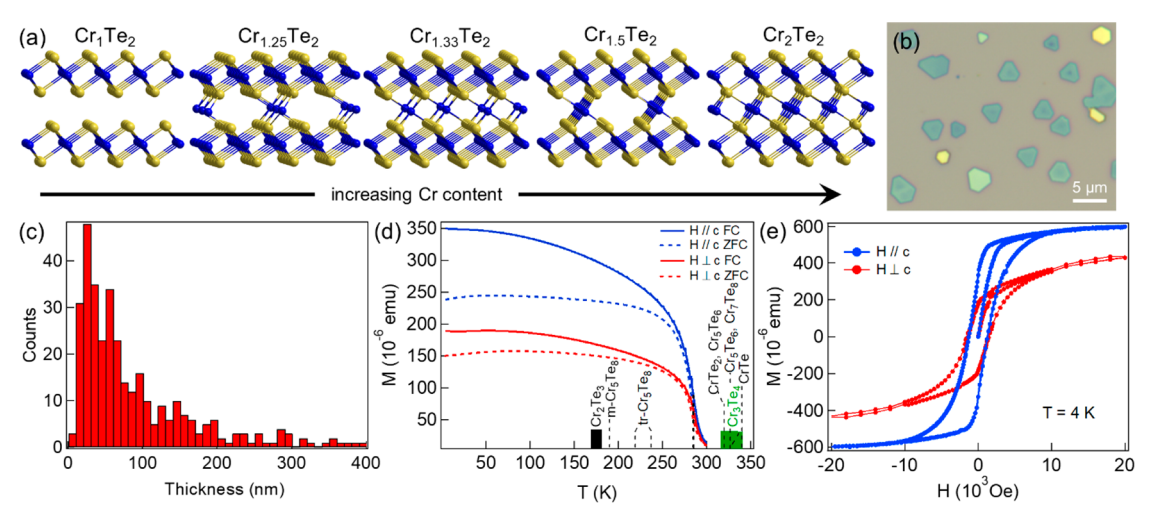


Figure 1. (a) The crystal structure of Cr_1Te_2 (Cr_2Te_2), $Cr_{1.25}Te_2$ (Cr_5Te_8), $Cr_{1.33}Te_2$ (Cr_2Te_3), $Cr_{1.5}Te_2$ (Cr_3Te_4), and Cr_2Te_2 (Cr_2Te_3); showing the difference between structures with the increase of intercalated Cr in the vdW gap between the Cr_2Te_2 layers, from left to right. (b) An optical image of a representative area of the chromium telluride nanoplates. (c) Histogram showing the range of thicknesses of nanoplates studied during the magnetization measurements. (d) M-T curves of the sample showing a T_c of \sim 284 K with the T_c of some known bulk chromium telluride compounds denoted along the horizontal axis. $^{35,47,62,63,65-67}$ (e) M-H curves of the sample with the field aligned perpendicular (red) and parallel (blue) to the c-axis at T=4 K.

Another interesting phenomenon reported in the CrTe₂based system is an anomalous thickness-dependent T_c which increases with decreasing thickness. 59,60 For example, Cr₂Te₃ (or $Cr_{1.33}Te_2$) in the bulk limit has a T_c of 160–180 K, whereas ultrathin nanoflakes (7.1 nm) have been reported to form ferromagnetic order at ~280 K. This thickness dependence is in strong contradiction to expectations based on the Mermin-Wagner-Hohenberg (MWH) theorem, which indicates that thermal fluctuations increase as dimensionality is reduced from 3D to 2D, therefore reducing the stability of the magnetic ordering and consequently lowering the ordering temper-It is worth mentioning, however, there are discrepancies in the literature regarding the magnetic properties of the same respective compounds. Indeed, varied T_c values were reported in the same compounds of similar thickness (e.g., $T_c = 210 \text{ K}^{59} \text{ versus } 300 \text{ K}^{32} \text{ for } \sim 9 \text{ nm thick}$ CrTe₂), and in contrast to the anomalous thickness dependence previously discussed, other studies (i.e., 1T-CrTe₂, Cr₃Te₄, and CrTe) suggested the absence of 34,35,57,62-64 or an opposite thickness dependence where the $T_{\rm c}$ decreases with decreasing thickness.³² Since magnetism in bulk $Cr_{1+\delta}Te_2$ is strongly dependent on the composition, $^{35,47,62,63,65-67}$ the varied and sometimes contrasting magnetic properties of nanoplates and thin films may result from precisely how the excess Cr atoms are intercalated in the vdW gap; therefore, it is essential to correlate the magnetic phases with the details of Cr-intercalation to understand the intrinsic magnetism in this newly emerged vdW magnet family.

In this work, we report on a ferromagnetic phase with a $T_{\rm c}$ of ~284 K in ${\rm Cr_{1+\delta}Te_2}$ nanoplates across a wide range of thicknesses from hundreds of nanometers down to 7 nm. An iterative method was developed, combining systematic transmission electron microscopy (TEM) measurements and simulations, to unambiguously determine the Cr-intercalation among 26,332 different possibilities. The Cr-intercalated structure identified in this process corresponds to a monoclinic ${\rm Cr_{1.5}Te_2}$ structure of space group ${\rm C2/m}$ which is segmented by vdW gaps, forming a vdW "superstructure". We also observed a twisted structure in the nanoplates, where the Cr-intercalated

layers are rotated by 120 degrees relative to one another. The vdW "superstructure" and twisting lead to magnetic properties in contrast to their bulk counterparts, which can be well understood based on the MWH theorem.

A single-step CVD growth, using CrCl₃ and Te as precursors (see experimental details in the Supporting Information), produces chromium telluride nanoplates of varied thickness down to 7 nm (Figure 1b,c). Magnetization measurements suggest a ferromagnetic $Cr_{1+\delta}Te_2$ phase with a magnetic ordering temperature $T_{\rm c}\sim 284$ K, in addition to the ${\rm Cr_2Te_3}$ (i.e., $\delta = 0.33$) phase with a $T_c \sim 170-177$ K as observed previously. 49 As shown in Figure 1d, the temperature dependent magnetization measurement was performed with an applied field oriented both parallel (H//c) and perpendicular $(H \perp c)$ to the c-axis for field-cooling (FC) and zero-field-cooling (ZFC). The T_c of 284 K, determined from $\frac{\mathrm{d} \mathrm{M}}{\mathrm{d} T}$, is different from the reported T_{c} values of any known bulk Cr_{1+δ}Te₂ compounds, as denoted along the horizontal axis in Figure 1d where the thicker lines indicate a range of reported T_c values for the respective compounds. 35,62,63,65–67 It is worth mentioning that ultrathin nanoplates (\sim 5-7 nm) grown by a similar CVD process, exhibit a magnetic transition at ~280 K and were believed to be Cr_2Te_3 (or $Cr_{1.33}Te_2$). Given that bulk Cr₂Te₃ has a T_c of 160-180 K, the enhanced ordering temperature in these ultrathin nanoplates was attributed to the reconstruction of structure. 60 This is, however, not the case in our nanoplates as the majority of them are in the range of 10-70 nm thick (Figure 1c), as characterized by atomic force microscopy. The magnetization measurements as a function of applied magnetic field (Figure 1e and Figure S1) show a rapid increase in the initial magnetization when the field is applied parallel to the c-axis compared to when the field is applied perpendicular to the c-axis, implying there is perpendicular magnetic anisotropy with the easy axis along the c-axis, which is common for many chromium tellurides. 32,49,64 Compared to Cr₂Te_{3,} which has a strong perpendicular magnetic anisotropy with an easy c-axis, ^{49,50} the perpendicular magnetic anisotropy on our nanoplates is relatively weak. Collectively, this

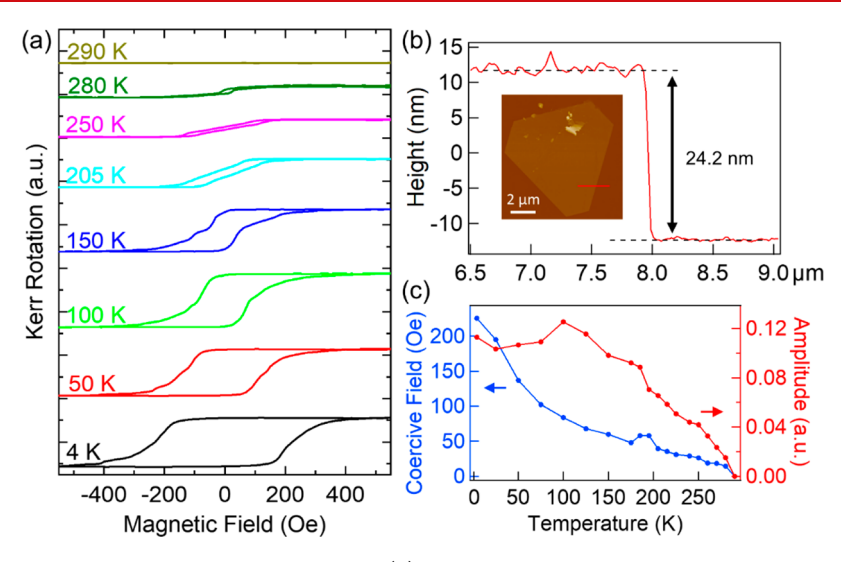


Figure 2. (a) MOKE hysteresis loops after background subtraction, (b) the AFM height profile with the corresponding AFM image in the inset, and (c) the coercive field of the Kerr rotation (blue) and amplitude as a function of temperature (red) on the same chromium telluride nanoplate.

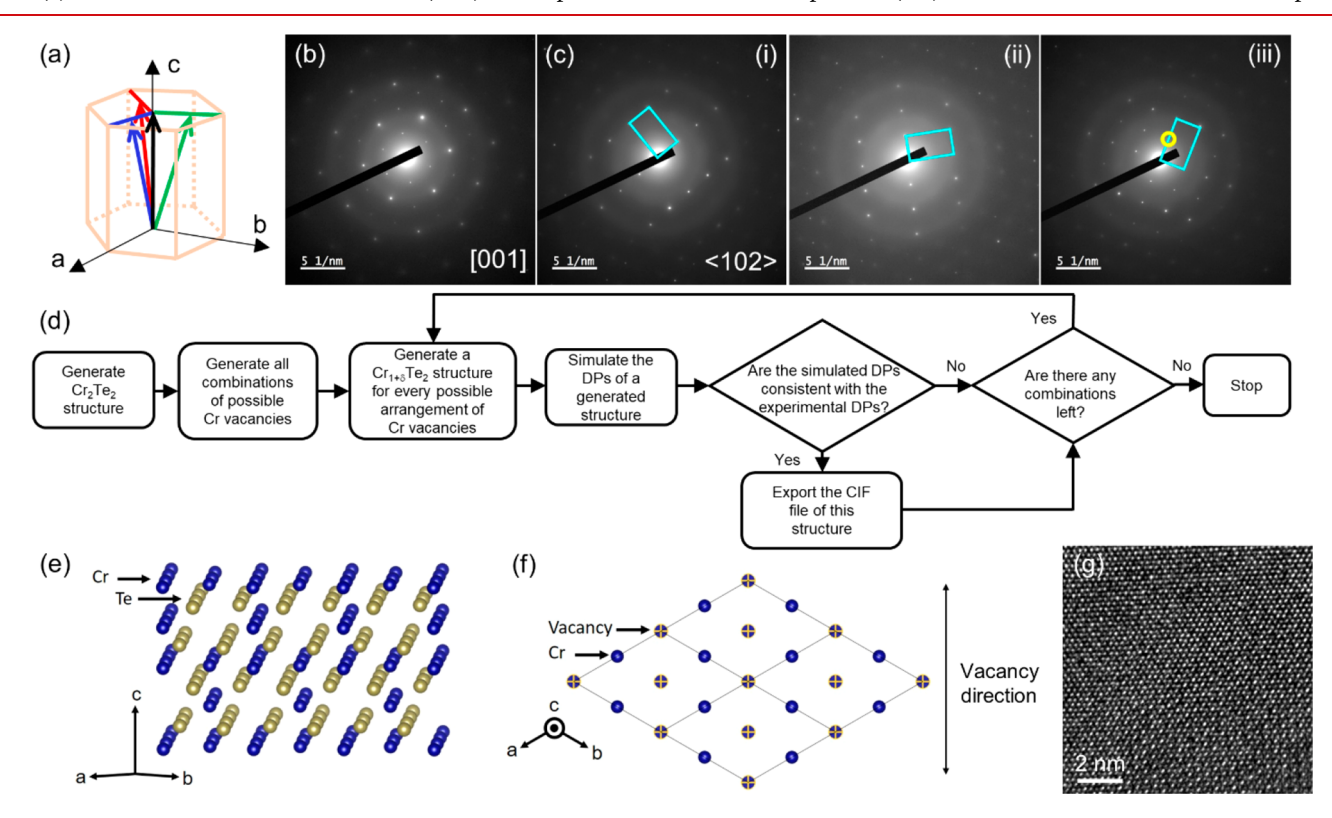


Figure 3. (a) Schematic figure of the [001] zone axis (black arrow) and the three $\langle 102 \rangle$ zone axes (colored arrows), (b) SAED pattern along the [001] zone axis, and (c) SAED patterns along three $\langle 102 \rangle$ zone axes, where extra diffraction spots are observed in one of the three zone axes. The extra spots are at the half of the diffraction vectors that are normal to the shortest diffraction vector along the $\langle 102 \rangle$ zone axis (one example is shown in a yellow circle). (d) The algorithm used to identify the structure of the chromium telluride nanoplates. (e) The side and (f) top views of the $Cr_{1.5}Te_2$ unit cell showing the positions of the vacancy sites. (g) HRTEM image of a nanoplate along the c-axis.

demonstrates that the nanoplates studied here are indeed a different phase of chromium telluride than Cr_2Te_3 . We note that there is a hysteresis loop at low fields along with a nonhysteretic and gradually increasing magnetization at higher fields in the $H \perp c$ loop; this is likely due to the nanoplates being randomly oriented in the in-plane direction where the measured M-H curve is the sum of individual curves of all nanoplates with the magnetic field applied along different in-

plane crystallographic axes, as described in the Supporting Information.

To demonstrate the intrinsic ferromagnetism and obtain the magnetic ordering temperatures of single nanoplates, we carried out magneto-optic Kerr effect (MOKE) measurements on some individual nanoplates at various temperatures between 4 and 300 K. The Kerr rotation was measured in the out-of-plane direction (i.e., along the *c*-axis) with the magnetic field applied out-of-plane, as well. The magnetic field

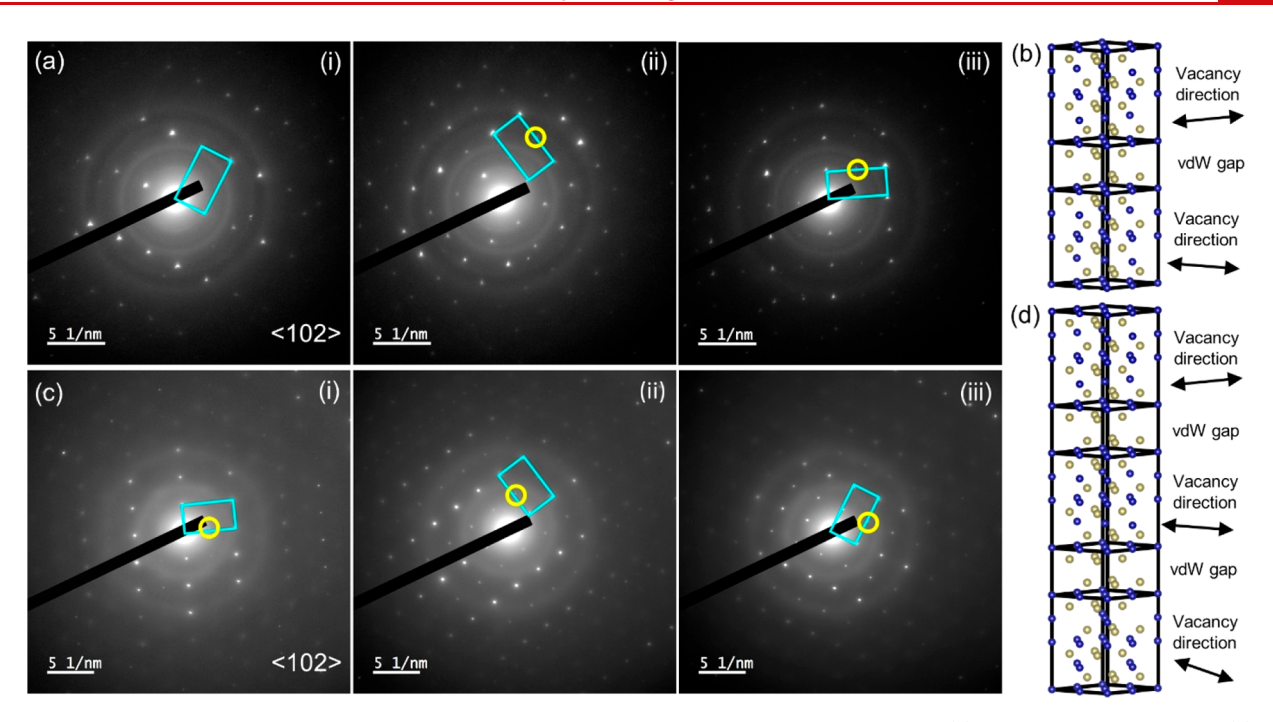


Figure 4. SAED patterns taken along three $\langle 102 \rangle$ zone axes where extra diffraction spots are observed in (a) two of the three axes and (c) in all three of the axes, indicated by the yellow circles, with the respective twisted structures shown in (b) and (d), respectively.

was swept between -600 Oe and +600 Oe. Figure 2a shows the magnetic field dependence of Kerr rotation taken on a 24.2 nm thick nanoplate (Figure 2b), in which magnetic hysteresis was observed from 4 to 280 K and disappeared by 290 K. The T_c is therefore determined to be 285 \pm 5 K, which is consistent with bulk measurements. The Kerr rotation amplitude and coercive field extracted from the magnetic hysteresis loops are plotted as a function of temperature in Figure 2c. It is worth noting that the Kerr rotation amplitude and coercive field are underestimated at low temperatures (e.g., ~100 K or below) due to the small sweeping field range which results in a measurement of minor loop in this temperature range. The same MOKE studies were performed on several other nanoplates of slightly different thicknesses (18.5 to 24.7 nm). As shown in Figure S8, we do not observe a systematic change in T_c as a function of thickness in this range.

Having demonstrated the intrinsic ferromagnetism in our nanoplates, we now turn to a systematic study of the Crintercalated crystal structure. As we have discussed in our previous work, 49 the c-lattice constants of various Crintercalated chromium tellurides vary only slightly between compounds, making it challenging to distinguish the different phases by standard X-ray diffraction characterization of dspacing along the out-of-plane c-axis when the nanoplates are lying flat on the substrate. We therefore carried out selected area electron diffraction (SAED) characterizations along different zone axes to gain both in-plane and out-of-plane structural information. As various intercalated phases can form during a CVD growth, ^{49,59} the SAED characterizations were taken on nine individual nanoplates from the same sample in which the magnetization measurements were performed to ensure the correlation of the structure and magnetism. It is worth noting that the nanoplates are sensitive to the electron beam (Figure S2 in the Supporting Information); thus a lower voltage (80 kV) was used during the SAED measurements to avoid damaging the nanoplates. As shown in Figure 3a, the

SAED patterns were taken along the [001] zone axis (denoted by a black arrow) and three adjacent (102) axes (colored arrows) which contain both in-plane and out-of-plane components. The diffraction pattern in the [001] zone axis (Figure 3b) can be indexed to CrTe2 as well as various Crintercalated phases including CrTe (Figure S4) which contains the maximum amount of Cr atoms intercalated in the vdW gap. While two of the [102] diffraction patterns (Figure 3c(i)-(ii) can also be assigned to the CrTe₂ structure (Figure S5), the third contains extra diffraction spots labeled by the circles in Figure 3c(iii). The extra diffraction spots were not due to electron-beam-induced damage as we performed SAED using a low voltage along three (102) axes and consequently repeated the measurement of the first [102] axis at the same tilt angle to confirm the SAED patterns remained unchanged (Figure S3). The observed extra diffraction spots are therefore intrinsic and likely associated with the Cr-intercalation in the vdW gap of the CrTe₂, which breaks the 3-fold lattice symmetry. We note that the observed SAED patterns measured along three of the (102) zone axes and the [001] axis were measured across the entirety of the nanoplate as well as in different regions of the nanoplate and are consistent with one another (Figure S6), indicating that the intercalated Cr atoms are ordered throughout the nanoplates. The high crystalline quality of the nanoplate is further confirmed by the high-resolution TEM (HRTEM) image in Figure 3g, which shows clear hexagonal lattice fringes.

To unambiguously determine how the Cr atoms are intercalated in the vdW gap, we developed an iterative method to search for the Cr-intercalated structure which matches the four observed SAED patterns. The extra diffraction spots in the [102] diffraction pattern (Figure 3c(iii)) exist at half of the reciprocal lattice vector of $CrTe_2$, indicating the Cr-intercalation sites double the period of the original $CrTe_2$ lattice. Furthermore, the structure of various Cr-intercalated $CrTe_2$ can also be described as Cr-vacated CrTe in which Cr

Nano Letters pubs.acs.org/NanoLett Letter

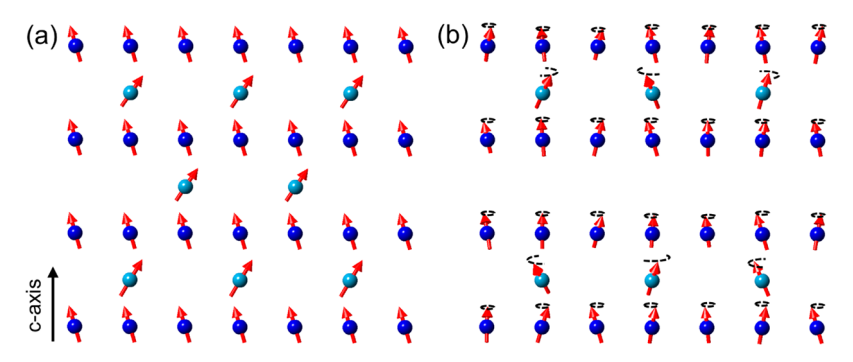


Figure 5. Side view of the fully occupied chromium layers (dark blue) and the self-intercalated chromium (light blue) vacancy layers showing orientations of magnetic moments. (a) Ground state configuration for coupled $Cr_{1.5}Te_2$ structure. (b) Decoupled $Cr_{1+\delta}Te_2$ superstructure with a vacant vdW gap. The dashed paths indicate the magnetic fluctuations that spoil the antiferromagnetic order in (a).

atoms have been partially removed from the vdW gap between CrTe₂ layers. Given that the vacancy sites are not limited to the gap between the CrTe₂ layers, Cr-vacated CrTe contains more possible lattice configurations than the Cr-intercalated CrTe₂; therefore to be more complementary, we used CrTe, instead of CrTe2, as a basis from which we generated Crvacated structures and respective diffraction patterns for comparison with the experimental data. The iterative algorithm we used to achieve this is described in Figure 3d. Since the unit cells of CrTe and CrTe2 are nearly the same size and are doubled by the Cr-intercalation (or vacancy), we first constructed a 2 × 2 × 2 supercell of CrTe consisting of 16 Cr atoms and 16 Te atoms. Next, we implemented a Python code to systematically remove n (n = 1, 2...7) Cr atoms at different positions from this super cell and consequently simulated all possible structures and respective diffraction patterns using the diffsims package from the pyxem opensource project.⁶⁸ Finally, we compared the simulated diffraction patterns to our experimental SAED data by indexing all of the diffraction spots that we observed and using them as inputs to be matched with the simulations in the iterative program, as described in the Supporting Information, from which the correct structure was determined.

Among 26,332 simulated structural phases, the only phase to match all of the diffraction patterns measured along the [001] and $\langle 102 \rangle$ zone axes (Figure 3b and c) is monoclinic $\mathrm{Cr}_{1.5}\mathrm{Te}_2$ of space group C2/m in which the 3-fold symmetry is broken. As shown in Figure 3e, the vdW gap between two $\mathrm{Cr}\mathrm{Te}_2$ layers is half filled with intercalated Cr atoms, where every second gap has oppositely occupied sites, resulting in a $\mathrm{Cr}_{1.5}\mathrm{Te}_2$ composition. As shown in the top view of the $\mathrm{Cr}_{1.5}\mathrm{Te}_2$ structure (Figure 3f), the unoccupied sites (i.e., vacancies) are distributed in the vdW gap along one of the three [100] directions, denoted as vacancy directions. The extra diffraction spots will appear along the [102] zone axis which has a finite component in this [100] vacancy direction.

Furthermore, we observed extra diffraction spots in the SAED patterns along two and/or all three of the $\langle 102 \rangle$ axes, as shown in Figures 4a,c, respectively. Of the 26,332 possible Crintercalated structures generated with the iterative method, none produced SAED patterns matching these observations. However, these exact SAED patterns can be generated by a twisted structure composed of the previously discussed $Cr_{1.5}Te_2$ layers when they are rotated by 120 degrees with respect to each other. For example, if the vacancies are distributed along the [100] direction in the bottom layers and along the [010] direction in the top layers (Figure 4b), then

the extra diffraction spots will appear in the diffraction patterns of both the [102] and [012] axes, as shown in Figure 4a. Similarly, in the case of a nanoplate which has a twisted structure with vacancies along all three $\langle 100 \rangle$ directions (Figure 4d), extra diffraction spots will appear in all three $\langle 102 \rangle$ axes as observed in Figure 4c. We note that while it is possible the $Cr_{1.5}Te_2$ layers segregate and form domains along the out-of-plane direction, we have confirmed that there exists a twisting between $Cr_{1.5}Te_2$ (either individual $Cr_{1.5}Te_2$ layers or $Cr_{1.5}Te_2$ domains) given that the extra spots we observe along two or three of the $\langle 102 \rangle$ zone axes do not match with any one of the nontwisted chromium telluride structures.

The stoichiometric ratio of the Cr_{1.5}Te₂ phase is calculated to be Cr/Te = 0.75. Surprisingly, X-ray energy-dispersive spectroscopy (XEDS), performed on the nanoplates where the SAED was taken, shows a Cr/Te ratio of ~0.59-0.68 (Figure S7), which is even lower than the ratio of $\sim 0.70-0.72$ measured on a Cr₂Te₃ control sample. While XEDS is a semiquantitative characterization method, a direct comparison of the nanoplates in this work and the control sample suggests that in addition to the Cr_{1.5}Te₂ phase the former may contain layers which are filled with fewer atoms in the vdW gap, resulting in a lower Cr/Te ratio than Cr_2Te_3 (i.e., $Cr_{10.7}Te_{16}$). 2 supercell are Cr₈Te₁₆, Cr₉Te₁₆, and Cr₁₀Te₁₆. The diffraction patterns produced by these layers must not contain any additional diffraction spots beyond what we observed (Figure 3b,c). As discussed earlier, the Cr₈Te₁₆ (i.e., CrTe₂) has a completely unoccupied vdW gap and produces diffraction patterns which agree with our observed patterns where extra spots are absent. Using our iterative algorithm, we further ruled out the other possibilities, i.e., $Cr_{10}Te_{16}$ and $Cr_{9}Te_{16}$, with the removal of 6 and 7 Cr atoms from the CrTe supercell, respectively. The above analysis therefore suggests that the Cr_{1.5}Te₂ is possibly segmented into layers, with completely empty vdW gaps separating them. This satisfies both the observed diffraction patterns and the measured Cr/Te ratio.

While direct imaging of the vdW gap using atomic-resolution STEM is challenging due to the high sensitivity of the sample to the e-beam, the observation of twisted $Cr_{1.5}Te_2$ layers supports the above segmentation scenario. Indeed, our density functional theory (DFT) calculation shows that the energy of the twisted $Cr_{1.5}Te_2$ system is lowered by the formation of the vdW gap between the twisted layers. In this calculation, we first modeled the twisted structure comprised of two 2 × 2 × 4 $Cr_{1.5}Te_2$ supercells with different vacancy directions, creating two $Cr_{1.5}Te_2$ — $Cr_{1.5}Te_2$ twist interfaces. A

second structure was then constructed by inserting a vdW gap between the two twisted Cr_{1.5}Te₂ supercells. The excess energy of the twisted $Cr_{1.5}Te_2-Cr_{1.5}Te_2$ interface is 59.1 mJ/m²; with a vdW gap, the excess energy was lowered to 17.4 mJ/m². Our DFT calculation therefore suggests that the twisted structure with a vdW gap is more energetically favorable. This result can be understood phenomenologically. In brief, the Cr_{1.5}Te₂ structures with vacancies along any of the three (100) vacancy directions are crystallographically equivalent with respect to the completely unoccupied vdW gap. Therefore, once a vdW gap is formed on top of the bottom Cr_{1.5}Te₂ layer, the orientation of the Cr_{1.5}Te₂ layer above the gap is not constrained by the bottom Cr_{1.5}Te₂; in other words, the vacancy directions of the two Cr_{1.5}Te₂ layers are decoupled by the vdW gap. For this reason, the Cr_{1.5}Te₂ layers in an individual nanoplate could have the same vacancy direction or be twisted by 120°, consistent with our experimental observation of the three cases.

The segmentation of Cr_{1.5}Te₂ by vdW gaps, which we call a vdW "superstructure", can result in magnetic properties that are distinct from bulk Cr_{1.5}Te₂ as shown in Figure 1d. The latter supports two magnetic transitions: one at 310 K associated with the easy axis ferromagnetism along the c-axis, and a second at 80 K associated with antiferromagnetism with a staggered magnetization developing between magnetic moments in the dilute and dense Cr layers which lie largely in the a-b plane (Figure 5a). ^{28,35} A simple model that captures this physics involves Heisenberg ferromagnetic couplings among spins within a plane and antiferromagnetic ones across planes, 40,41 as well as an easy-axis anisotropy in the dense layers and easy-plane anisotropy in the dilute planes. In meanfield theory, the ground state magnetic ordering involves canted spins with two broken symmetries: one Ising-like, representing ferromagnetic order along the c-axis, and one XYlike, involving the in-plane ordering of the staggered magnetization. The latter is characterized by a broken continuous U(1) symmetry, and therefore is much more susceptible to thermal fluctuations than the former, with a phase transition expected to fall in the three-dimensional XY universality class. The easy-axis anisotropy supports the broken Z_2 symmetry of the ferromagnetic state to a higher temperature and thermally disorders via a transition in the threedimensional Ising universality class. The presence of completely empty vdW gaps breaks up the magnetic system into a stack of essentially two-dimensional Cr_{1.5}Te₂ layers. Because of the Mermin-Wagner theorem, 27 thermal fluctuations eliminate U(1) long-range ordering at any nonvanishing temperature so that the low-temperature phase transition seen in bulk Cr_{1.5}Te₂ systems is eliminated. (Note that this assumes perfect XY spin isotropy with gapless spin waves. The model however accommodates some anisotropy provided the resulting gap is well below experimental temperatures.) Moreover, due to the generally stronger effects of thermal fluctuations in lower dimensions, as well as the reduced number of Heisenberg bonds interconnecting the magnetic moments in the system as a whole, one expects the ferromagnetic ordering temperature to be reduced relative to bulk Cr_{1.5}Te₂ (Figure 5b). The twisting further suppresses the couplings between the Cr_{1.5}Te₂ layers and therefore the magnetic ordering temperatures.

In summary, we have demonstrated the structural twisting and segmentation in self-intercalated $Cr_{1+\delta}Te_2$ nanoplates using a newly developed iterative method which combines

systematic electron diffraction measurements and structural simulations. Among 26,332 possible structural configurations, we unambiguously identified the Cr-intercalated structure as 3fold symmetry broken Cr_{1.5}Te₂ layers which are segmented by vdW gaps. Moreover, a twisted structure is observed where the Cr_{1.5}Te₂ layers are rotated by 120°. The segmentation and twisting lead to a slight reduction of the ferromagnetic transition temperature and destroys the antiferromagnetic order at a finite temperature, whereas the perpendicular ferromagnetism is preserved. Given the contrasting magnetic properties reported in the chromium telluride family, our work highlights the importance of precisely pinpointing the intercalated structures to correctly attribute the intrinsic magnetism in this newly emerged vdW magnet with roomtemperature ferromagnetism. The iterative method developed in this work offers a more streamlined approach to characterizing the self-intercalation in 2D vdW materials without the need for atomically resolved cross-sectional TEM studies, which is especially useful when the sample is sensitive to an ebeam, such as this case. The spontaneous formation of a vdW superstructure not only provides insight into the diverse and engineerable magnetic properties of intercalated vdW magnets but may also add complementary building blocks to vdWbased spintronics.

ASSOCIATED CONTENT

Supporting Information

The Supporting Information is available free of charge at https://pubs.acs.org/doi/10.1021/acs.nanolett.1c02940.

Experimental and calculation details; preparation of samples for magnetization measurement and AFM details; M–H loops at various temperatures; nanoplate sensitivity to the electron beam; simulated diffraction patterns of various chromium tellurides; SAED patterns demonstrating consistent structure in different regions of the nanoplates; Cr/Te ratios of nanoplates determined from STEM-XEDS as a function of the number of $\langle 102 \rangle$ diffraction patterns with extra diffraction spots; H_c determined from the MOKE measurements as a function of temperature (PDF)

AUTHOR INFORMATION

Corresponding Author

Shixiong Zhang — Department of Physics and Quantum Science and Engineering Center, Indiana University, Bloomington, Indiana 47405, United States; o orcid.org/0000-0002-1004-0597; Email: sxzhang@indiana.edu

Authors

Amanda L. Coughlin – Department of Physics, Indiana University, Bloomington, Indiana 47405, United States Dongyue Xie – Department of Mechanical and Materials Engineering, University of Nebraska, Lincoln, Nebraska 68588, United States

Xun Zhan — Electron Microscope Center, Indiana University, Bloomington, Indiana 47405, United States

Yue Yao – Department of Physics and Astronomy, University of Utah, Salt Lake City, Utah 84112, United States

Liangzi Deng – Texas Center for Superconductivity and Department of Physics, University of Houston, Houston, Texas 77204, United States

- Heshan Hewa-Walpitage Department of Physics and Astronomy, University of Utah, Salt Lake City, Utah 84112, United States
- Trevor Bontke Texas Center for Superconductivity and Department of Physics, University of Houston, Houston, Texas 77204, United States
- Ching-Wu Chu Texas Center for Superconductivity and Department of Physics, University of Houston, Houston, Texas 77204, United States; Lawrence Berkeley National Laboratory, Berkeley, California 94720, United States; orcid.org/0000-0003-3955-7095
- Yan Li Department of Physics and Astronomy, University of Utah, Salt Lake City, Utah 84112, United States
- Jian Wang Department of Mechanical and Materials Engineering, University of Nebraska, Lincoln, Nebraska 68588, United States
- Herbert A. Fertig Department of Physics and Quantum Science and Engineering Center, Indiana University, Bloomington, Indiana 47405, United States

Complete contact information is available at: https://pubs.acs.org/10.1021/acs.nanolett.1c02940

Author Contributions

OA.C., D.X., and X.Z. contributed equally to this work.

The authors declare no competing financial interest.

ACKNOWLEDGMENTS

We acknowledge support from the U.S. National Science foundation through Grants ECCS-1936406 and DMR-1914451. Further support was supplied by the U.S.-Israel Binational Science Foundation Grant 2016130. H.A.F. acknowledges the support of the Research Corporation for Science Advancement through a Cottrell SEED Award. The electron microscopy studies performed in the Nebraska Center for Materials and Nanoscience was supported by the National Science Foundation under Award ECCS: 1542182 and the Nebraska Research Initiative. Atomistic simulations were completed utilizing the Holland Computing Center of the University of Nebraska, which receives support from the Nebraska Research Initiative. The work performed at the Texas Center of Superconductivity at the University of Houston is supported by U.S. Air Force Office of Scientific Research Grants FA9550-15-1-0236 and FA9550-20-1-0068, the T. L. L. Temple Foundation, the John J. and Rebecca Moores Endowment, and the State of Texas through the Texas Center for Superconductivity at the University of Houston. We thank the Indiana University-Bloomington Electron Microscopy Center for access to transmission electron microscope and Nanoscale Characterization Facility for access to atomic force microscope.

REFERENCES

- (1) Gong, C.; Li, L.; Li, Z.; Ji, H.; Stern, A.; Xia, Y.; Cao, T.; Bao, W.; Wang, C.; Wang, Y.; Qiu, Z. Q.; Cava, R. J.; Louie, S. G.; Xia, J.; Zhang, X. Discovery of Intrinsic Ferromagnetism in Two-Dimensional Van Der Waals Crystals. *Nature* **2017**, *546* (7657), 265–269.
- (2) Huang, B.; Clark, G.; Navarro-Moratalla, E.; Klein, D. R.; Cheng, R.; Seyler, K. L.; Zhong, D.; Schmidgall, E.; McGuire, M. A.; Cobden, D. H.; Yao, W.; Xiao, D.; Jarillo-Herrero, P.; Xu, X. Layer-Dependent Ferromagnetism in a Van Der Waals Crystal Down to the Monolayer Limit. *Nature* **2017**, *546* (7657), 270–273.

- (3) Burch, K. S.; Mandrus, D.; Park, J.-G. Magnetism in Two-Dimensional Van Der Waals Materials. *Nature* **2018**, *563* (7729), 47–52.
- (4) Gibertini, M.; Koperski, M.; Morpurgo, A.; Novoselov, K. Magnetic 2d Materials and Heterostructures. *Nat. Nanotechnol.* **2019**, *14* (5), 408–419.
- (5) Mak, K. F.; Shan, J.; Ralph, D. C. Probing and Controlling Magnetic States in 2d Layered Magnetic Materials. *Nature Reviews Physics* **2019**, *1* (11), 646–661.
- (6) Huang, B.; McGuire, M. A.; May, A. F.; Xiao, D.; Jarillo-Herrero, P.; Xu, X. Emergent Phenomena and Proximity Effects in Two-Dimensional Magnets and Heterostructures. *Nat. Mater.* **2020**, *19* (12), 1276–1289.
- (7) Kawakami, R. K. Spin and Magnetism in 2d Materials. *arxiv* (Mesoscale and Nanoscale Physics, Materials Science), Nov. 3, 2019. https://arxiv.org/abs/1911.00894 (accessed 2021-07-21).
- (8) Li, H.; Ruan, S. C.; Zeng, Y. J. Intrinsic Van Der Waals Magnetic Materials from Bulk to the 2d Limit: New Frontiers of Spintronics. *Adv. Mater.* **2019**, *31* (27), 1900065.
- (9) Carcia, P.; Meinhaldt, A.; Suna, A. Perpendicular Magnetic Anisotropy in Pd/Co Thin Film Layered Structures. *Appl. Phys. Lett.* **1985**, 47 (2), 178–180.
- (10) Huang, F.; Kief, M.; Mankey, G.; Willis, R. Magnetism in the Few-Monolayers Limit: A Surface Magneto-Optic Kerr-Effect Study of the Magnetic Behavior of Ultrathin Films of Co, Ni, and Co-Ni Alloys on Cu (100) and Cu (111). *Phys. Rev. B: Condens. Matter Mater. Phys.* **1994**, 49 (6), 3962–3971.
- (11) Geim, A. K.; Grigorieva, I. V. Van Der Waals Heterostructures. *Nature* **2013**, 499 (7459), 419–425.
- (12) Jiang, S.; Shan, J.; Mak, K. F. Electric-Field Switching of Two-Dimensional Van Der Waals Magnets. *Nat. Mater.* **2018**, *17* (5), 406–410.
- (13) Huang, B.; Clark, G.; Klein, D. R.; MacNeill, D.; Navarro-Moratalla, E.; Seyler, K. L.; Wilson, N.; McGuire, M. A.; Cobden, D. H.; Xiao, D.; Yao, W.; Jarillo-Herrero, P.; Xu, X. Electrical Control of 2d Magnetism in Bilayer Cri 3. *Nat. Nanotechnol.* **2018**, *13* (7), 544–548.
- (14) Xing, W.; Chen, Y.; Odenthal, P. M.; Zhang, X.; Yuan, W.; Su, T.; Song, Q.; Wang, T.; Zhong, J.; Jia, S.; Xie, X. C.; Li, Y. S.; Han, W. Electric Field Effect in Multilayer Cr2ge2te6: A Ferromagnetic 2d Material. 2D Mater. 2017, 4 (2), 024009.
- (15) Liu, J.; Sun, Q.; Kawazoe, Y.; Jena, P. Exfoliating Biocompatible Ferromagnetic Cr-Trihalide Monolayers. *Phys. Chem. Chem. Phys.* **2016**, *18* (13), 8777–8784.
- (16) Jiang, S.; Li, L.; Wang, Z.; Mak, K. F.; Shan, J. Controlling Magnetism in 2d Cri 3 by Electrostatic Doping. *Nat. Nanotechnol.* **2018**, *13* (7), 549–553.
- (17) Georgiou, T.; Jalil, R.; Belle, B. D.; Britnell, L.; Gorbachev, R. V.; Morozov, S. V.; Kim, Y.-J.; Gholinia, A.; Haigh, S. J.; Makarovsky, O.; Eaves, L.; Ponomarenko, L. A.; Geim, A. K.; Novoselov, K. S.; Mishchenko, A. Vertical Field-Effect Transistor Based on Graphene—Ws 2 Heterostructures for Flexible and Transparent Electronics. *Nat. Nanotechnol.* **2013**, 8 (2), 100–103.
- (18) Sarkar, D.; Xie, X.; Liu, W.; Cao, W.; Kang, J.; Gong, Y.; Kraemer, S.; Ajayan, P. M.; Banerjee, K. A Subthermionic Tunnel Field-Effect Transistor with an Atomically Thin Channel. *Nature* **2015**, 526 (7571), 91–95.
- (19) Song, T.; Cai, X.; Tu, M. W.-Y.; Zhang, X.; Huang, B.; Wilson, N. P.; Seyler, K. L.; Zhu, L.; Taniguchi, T.; Watanabe, K.; McGuire, M. A.; Cobden, D. H.; Xiao, D.; Yao, W.; Xu, X. Giant Tunneling Magnetoresistance in Spin-Filter Van Der Waals Heterostructures. *Science* 2018, 360 (6394), 1214–1218.
- (20) Kim, H. H.; Yang, B.; Patel, T.; Sfigakis, F.; Li, C.; Tian, S.; Lei, H.; Tsen, A. W. One Million Percent Tunnel Magnetoresistance in a Magnetic Van Der Waals Heterostructure. *Nano Lett.* **2018**, *18* (8), 4885–4890.
- (21) Wang, Z.; Gutiérrez-Lezama, I.; Ubrig, N.; Kroner, M.; Gibertini, M.; Taniguchi, T.; Watanabe, K.; Imamoğlu, A.; Giannini, E.; Morpurgo, A. F. Very Large Tunneling Magnetoresistance in

- Layered Magnetic Semiconductor Cri 3. Nat. Commun. 2018, 9 (1), 1–8.
- (22) Jiang, S.; Li, L.; Wang, Z.; Shan, J.; Mak, K. F. Spin Tunnel Field-Effect Transistors Based on Two-Dimensional Van Der Waals Heterostructures. *Nature Electronics* **2019**, 2 (4), 159–163.
- (23) Lado, J. L.; Fernández-Rossier, J. On the Origin of Magnetic Anisotropy in Two Dimensional Cri3. 2D Mater. 2017, 4 (3), 035002.
- (24) Sivadas, N.; Okamoto, S.; Xu, X.; Fennie, C. J.; Xiao, D. Stacking-Dependent Magnetism in Bilayer Cri3. *Nano Lett.* **2018**, *18* (12), 7658–7664.
- (25) McCreary, A.; Mai, T. T.; Utermohlen, F. G.; Simpson, J. R.; Garrity, K. F.; Feng, X.; Shcherbakov, D.; Zhu, Y.; Hu, J.; Weber, D.; Watanabe, K.; Taniguchi, T.; Goldberger, J. E.; Mao, Z.; Lau, C. N.; Lu, Y.; Trivedi, N.; Valdes Aguilar, R.; Hight Walker, A. R. Distinct Magneto-Raman Signatures of Spin-Flip Phase Transitions in Cri3. *Nat. Commun.* 2020, 11 (1), 1–8.
- (26) Jiang, P.; Wang, C.; Chen, D.; Zhong, Z.; Yuan, Z.; Lu, Z.-Y.; Ji, W. Stacking Tunable Interlayer Magnetism in Bilayer Cri 3. *Phys. Rev. B: Condens. Matter Mater. Phys.* **2019**, *99* (14), 144401.
- (27) Ghazaryan, D.; Greenaway, M. T.; Wang, Z.; Guarochico-Moreira, V. H.; Vera-Marun, I. J.; Yin, J.; Liao, Y.; Morozov, S. V.; Kristanovski, O.; Lichtenstein, A. I.; Katsnelson, M. I.; Withers, F.; Mishchenko, A.; Eaves, L.; Geim, A. K.; Novoselov, K. S.; Misra, A. Magnon-Assisted Tunnelling in Van Der Waals Heterostructures Based on Crbr3. *Nature Electronics* **2018**, *1* (6), 344–349.
- (28) Chen, W. O.; Sun, Z. Y.; Wang, Z. J.; Gu, L. H.; Xu, X. D.; Wu, S. W.; Gao, C. L. Direct Observation of Van Der Waals Stacking-Dependent Interlayer Magnetism. *Science* **2019**, *366* (6468), 983–987.
- (29) Zhang, Z. W.; Shang, J. Z.; Jiang, C. Y.; Rasmita, A.; Gao, W. B.; Yu, T. Direct Photoluminescence Probing of Ferromagnetism in Monolayer Two-Dimensional Crbr3. *Nano Lett.* **2019**, *19* (5), 3138–3142.
- (30) Soriano, D.; Katsnelson, M. I.; Fernandez-Rossier, J. Magnetic Two-Dimensional Chromium Trihalides: A Theoretical Perspective. *Nano Lett.* **2020**, 20 (9), 6225–6234.
- (31) Shcherbakov, D.; Stepanov, P.; Weber, D.; Wang, Y.; Hu, J.; Zhu, Y.; Watanabe, K.; Taniguchi, T.; Mao, Z.; Windl, W.; Goldberger, J. E.; Bockrath, M.; Lau, C. N. Raman Spectroscopy, Photocatalytic Degradation, and Stabilization of Atomically Thin Chromium Tri-Iodide. *Nano Lett.* **2018**, *18* (7), 4214–4219.
- (32) Zhang, X.; Lu, Q.; Liu, W.; Niu, W.; Sun, J.; Cook, J.; Vaninger, M.; Miceli, P. F.; Singh, D. J.; Lian, S.-W.; Chang, T.-R.; He, X.; Du, J.; He, L.; Zhang, R.; Bian, G.; Xu, Y. Room-Temperature Intrinsic Ferromagnetism in Epitaxial Crte 2 Ultrathin Films. *Nat. Commun.* **2021**, *12* (1), 1–9.
- (33) Huang, M.; Wang, S.; Wang, Z.; Liu, P.; Xiang, J.; Feng, C.; Wang, X.; Zhang, Z.; Wen, Z.; Xu, H.; Yu, G.; Lu, Y.; Zhao, W.; Yang, S. A.; Hou, D.; Xiang, B. Colossal Anomalous Hall Effect in Ferromagnetic Van Der Waals Crte2. *ACS Nano* **2021**, *15*, 9759–9763.
- (34) Sun, X.; Li, W.; Wang, X.; Sui, Q.; Zhang, T.; Wang, Z.; Liu, L.; Li, D.; Feng, S.; Zhong, S.; Wang, H.; Bouchiat, V.; Nunez Regueiro, M.; Rougemaille, N.; Coraux, J.; Purbawati, A.; Hadj-Azzem, A.; Wang, Z.; Dong, B.; Wu, X.; Yang, T.; Yu, G.; Wang, B.; Han, Z.; Han, X.; Zhang, Z. Room Temperature Ferromagnetism in Ultra-Thin Van Der Waals Crystals of 1t-Crte2. *Nano Res.* **2020**, *13* (12), 3358–3363.
- (35) Freitas, D. C.; Weht, R.; Sulpice, A.; Remenyi, G.; Strobel, P.; Gay, F.; Marcus, J.; Núñez-Regueiro, M. Ferromagnetism in Layered Metastable 1t-Crte2. *J. Phys.: Condens. Matter* 2015, 27 (17), 176002. (36) Purbawati, A.; Coraux, J.; Vogel, J.; Hadj-Azzem, A.; Wu, N. J.; Bendiab, N.; Jegouso, D.; Renard, J.; Marty, L.; Bouchiat, V.; Sulpice, A.; Aballe, L.; Foerster, M.; Genuzio, F.; Locatelli, A.; Mentes, T. O.; Han, Z. V.; Sun, X. D.; Nunez-Regueiro, M.; Rougemaille, N. In-Plane Magnetic Domains and Neel-Like Domain Walls in Thin Flakes of the Room Temperature Crte2 Van Der Waals Ferromagnet. *ACS Appl. Mater. Interfaces* 2020, 12 (27), 30702–30710.

- (37) Carteaux, V.; Moussa, F.; Spiesser, M. 2d Ising-Like Ferromagnetic Behaviour for the Lamellar Cr2si2te6 Compound: A Neutron Scattering Investigation. *Europhys. Lett.* **1995**, 29 (3), 251–256.
- (38) Wang, Z.; Zhang, T.; Ding, M.; Dong, B.; Li, Y.; Chen, M.; Li, X.; Huang, J.; Wang, H.; Zhao, X.; Li, Y.; Li, D.; Jia, C.; Sun, L.; Guo, H.; Ye, Y.; Sun, D.; Chen, Y.; Yang, T.; Zhang, J.; et al. Electric-Field Control of Magnetism in a Few-Layered Van Der Waals Ferromagnetic Semiconductor. *Nat. Nanotechnol.* **2018**, *13* (7), 554–559.
- (39) Tian, Y.; Gray, M. J.; Ji, H.; Cava, R.; Burch, K. S. Magneto-Elastic Coupling in a Potential Ferromagnetic 2d Atomic Crystal. 2D Mater. 2016, 3 (2), 025035.
- (40) Williams, T. J.; Aczel, A. A.; Lumsden, M. D.; Nagler, S. E.; Stone, M. B.; Yan, J.-Q.; Mandrus, D. Magnetic Correlations in the Quasi-Two-Dimensional Semiconducting Ferromagnet Crsite 3. *Phys. Rev. B: Condens. Matter Mater. Phys.* **2015**, 92 (14), 144404.
- (41) Liu, Y.; Petrovic, C. Critical Behavior of Quasi-Two-Dimensional Semiconducting Ferromagnet Cr 2 Ge 2 Te 6. *Phys. Rev. B: Condens. Matter Mater. Phys.* **2017**, *96* (5), 054406.
- (42) Casto, L. D.; Clune, A. J.; Yokosuk, M. O.; Musfeldt, J. L.; Williams, T. J.; Zhuang, H. L.; Lin, M.-W.; Xiao, K.; Hennig, R. G.; Sales, B. C.; Yan, J.-Q.; Mandrus, D. Strong Spin-Lattice Coupling in Crsite3. *APL Mater.* **2015**, *3* (4), 041515.
- (43) Lohmann, M.; Su, T.; Niu, B.; Hou, Y.; Alghamdi, M.; Aldosary, M.; Xing, W.; Zhong, J.; Jia, S.; Han, W.; Wu, R.; Cui, Y.-T.; Shi, J. Probing Magnetism in Insulating Cr2ge2te6 by Induced Anomalous Hall Effect in Pt. *Nano Lett.* **2019**, *19* (4), 2397–2403.
- (44) Liu, Y.; Petrovic, C. Anisotropic Magnetic Entropy Change in Cr2 × 2te6 (X = Si and Ge). *Phys, Rev. Mater.* **2019**, 3 (1), 014001.
- (45) Huang, M.; Ma, Z.; Wang, S.; Li, S.; Li, M.; Xiang, J.; Liu, P.; Hu, G.; Zhang, Z.; Sun, Z.; Lu, Y.; Sheng, Z.; Chen, G.; Chueh, Y.-L.; Yang, S. A.; Xiang, B. Significant Perpendicular Magnetic Anisotropy in Room-Temperature Layered Ferromagnet of Cr-Intercalated Crte2. 2D Mater. 2021, 8 (3), 031003.
- (46) Liu, Y.; Petrovic, C. Critical Behavior of the Quasi-Two-Dimensional Weak Itinerant Ferromagnet Trigonal Chromium Telluride Cr 0.62 Te. *Phys. Rev. B: Condens. Matter Mater. Phys.* **2017**, 96 (13), 134410.
- (47) Liu, Y.; Petrovic, C. Anomalous Hall Effect in the Trigonal Cr 5 Te 8 Single Crystal. *Phys. Rev. B: Condens. Matter Mater. Phys.* **2018**, 98 (19), 195122.
- (48) Liu, Y.; Abeykoon, M.; Stavitski, E.; Attenkofer, K.; Petrovic, C. Magnetic Anisotropy and Entropy Change in Trigonal Cr 5 Te 8. *Phys. Rev. B: Condens. Matter Mater. Phys.* **2019**, *100* (24), 245114.
- (49) Coughlin, A. L.; Xie, D.; Yao, Y.; Zhan, X.; Chen, Q.; Hewa-Walpitage, H.; Zhang, X.; Guo, H.; Zhou, H.; Lou, J.; Wang, J.; Li, Y. S.; Fertig, H. A.; Zhang, S. Near Degeneracy of Magnetic Phases in Two-Dimensional Chromium Telluride with Enhanced Perpendicular Magnetic Anisotropy. ACS Nano 2020, 14 (11), 15256–15266.
- (50) Roy, A.; Guchhait, S.; Dey, R.; Pramanik, T.; Hsieh, C.-C.; Rai, A.; Banerjee, S. K. Perpendicular Magnetic Anisotropy and Spin Glass-Like Behavior in Molecular Beam Epitaxy Grown Chromium Telluride Thin Films. *ACS Nano* **2015**, *9* (4), 3772–3779.
- (51) Wang, M.; Kang, L.; Su, J.; Zhang, L.; Dai, H.; Cheng, H.; Han, X.; Zhai, T.; Liu, Z.; Han, J. Two-Dimensional Ferromagnetism in Crte Flakes Down to Atomically Thin Layers. *Nanoscale* **2020**, *12* (31), 16427–16432.
- (52) Luo, X.-H.; Ren, W.-J.; Zhang, Z.-D. Magnetic Properties and Magnetocaloric Effect of a Trigonal Te-Rich CrSte8 Single Crystal. *J. Magn. Magn. Mater.* **2018**, *445*, 37–43.
- (53) Wang, F.; Du, J.; Sun, F.; Sabirianov, R. F.; Al-Aqtash, N.; Sengupta, D.; Zeng, H.; Xu, X. Ferromagnetic Cr 2 Te 3 Nanorods with Ultrahigh Coercivity. *Nanoscale* **2018**, *10* (23), 11028–11033.
- (54) Burn, D. M.; Duffy, L.; Fujita, R.; Zhang, S.; Figueroa, A. I.; Herrero-Martin, J.; Van Der Laan, G.; Hesjedal, T. Cr 2 Te 3 Thin Films for Integration in Magnetic Topological Insulator Heterostructures. *Sci. Rep.* **2019**, *9* (1), 1–10.

- (55) Li, H.; Wang, L.; Chen, J.; Yu, T.; Zhou, L.; Qiu, Y.; He, H.; Ye, F.; Sou, I. K.; Wang, G. Molecular Beam Epitaxy Grown Cr2te3 Thin Films with Tunable Curie Temperatures for Spintronic Devices. *ACS Appl. Nano Mater.* **2019**, *2* (11), 6809–6817.
- (56) Zhang, L.-Z.; He, X.-D.; Zhang, A.-L.; Xiao, Q.-L.; Lu, W.-L.; Chen, F.; Feng, Z.; Cao, S.; Zhang, J.; Ge, J.-Y. Tunable Curie Temperature in Layered Ferromagnetic Cr5+Xte8 Single Crystals. *APL Mater.* **2020**, 8 (3), 031101.
- (57) Zhao, D.; Zhang, L.; Malik, I. A.; Liao, M.; Cui, W.; Cai, X.; Zheng, C.; Li, L.; Hu, X.; Zhang, D.; Zhang, J.; Chen, X.; Jiang, W.; Xue, Q. Observation of Unconventional Anomalous Hall Effect in Epitaxial Crte Thin Films. *Nano Res.* **2018**, *11* (6), 3116–3121.
- (58) Zhou, L.; Chen, J. S.; Chen, X. B.; Xi, B.; Qiu, Y.; Zhang, J. W.; Wang, L. J.; Zhang, R. N.; Ye, B. C.; Chen, P. B.; Zhang, X. X.; Guo, G. P.; Yu, D. P.; Mei, J. W.; Ye, F.; Wang, G.; He, H. T. Topological Hall Effect in Traditional Ferromagnet Embedded with Black-Phosphorus-Like Bismuth Nanosheets. ACS Appl. Mater. Interfaces 2020, 12 (22), 25135–25142.
- (59) Meng, L.; Zhou, Z.; Xu, M.; Yang, S.; Si, K.; Liu, L.; Wang, X.; Jiang, H.; Li, B.; Qin, P.; Zhang, P.; Wang, J.; Liu, Z.; Tang, P.; Ye, Y.; Zhou, W.; Bao, L.; Gao, H.-J.; Gong, Y. Anomalous Thickness Dependence of Curie Temperature in Air-Stable Two-Dimensional Ferromagnetic 1t-Crte 2 Grown by Chemical Vapor Deposition. *Nat. Commun.* 2021, 12 (1), 1–8.
- (60) Wen, Y.; Liu, Z.; Zhang, Y.; Xia, C.; Zhai, B.; Zhang, X.; Zhai, G.; Shen, C.; He, P.; Cheng, R.; Yin, L.; Yao, Y.; Getaye Sendeku, M.; Wang, Z.; Ye, X.; Liu, C.; Jiang, C.; Shan, C.; Long, Y.; He, J. Tunable Room-Temperature Ferromagnetism in Two-Dimensional Cr2te3. *Nano Lett.* **2020**, 20 (5), 3130–3139.
- (61) Mermin, N. D.; Wagner, H. Absence of Ferromagnetism or Antiferromagnetism in One-or Two-Dimensional Isotropic Heisenberg Models. *Phys. Rev. Lett.* **1966**, *17* (22), 1133–1136.
- (62) Andresen, A. F.; Zeppezauer, E.; Boive, T.; Nordstrom, B.; Branden, C.-I. Magnetic Structure of Cr2te3, Cr3te4, and Cr5te6. *Acta Chem. Scand.* 1970, 24 (10), 3495–3509.
- (63) Dijkstra, J; Weitering, H H; Bruggen, C F v.; Haas, C; Groot, R A d. Band-Structure Calculations, and Magnetic and Transport Properties of Ferromagnetic Chromium Tellurides (Crte, Cr3te4, Cr2te3). J. Phys.: Condens. Matter 1989, 1 (46), 9141–9161.
- (64) Chua, R.; Zhou, J.; Yu, X. J.; Yu, W.; Gou, J.; Zhu, R.; Zhang, L.; Liu, M. Z.; Breese, M. B. H.; Chen, W.; Loh, K. P.; Feng, Y. P.; Yang, M.; Huang, Y. L.; Wee, A. T. S. Room Temperature Ferromagnetism of Monolayer Chromium Telluride with Perpendicular Magnetic Anisotropy. *Adv. Mater.* 2021, 33 (42), 2103360.
- (65) Lukoschus, K.; Kraschinski, S.; Näther, C.; Bensch, W.; Kremer, R. Magnetic Properties and Low Temperature X-Ray Studies of the Weak Ferromagnetic Monoclinic and Trigonal Chromium Tellurides Cr5te8. *J. Solid State Chem.* **2004**, *177* (3), 951–959.
- (66) Shimada, K.; Saitoh, T.; Namatame, H.; Fujimori, A.; Ishida, S.; Asano, S.; Matoba, M.; Anzai, S. Photoemission Study of Itinerant Ferromagnet Cr1 $-\Delta$ te. *Phys. Rev. B: Condens. Matter Mater. Phys.* **1996**, 53 (12), 7673-7683.
- (67) Akram, M.; Nazar, F. M. Magnetic Properties of Crte, Cr 23 Te 24, Cr 7 Te 8, Cr 5 Te 6, and Cr 3 Te 4 Compounds. *J. Mater. Sci.* **1983**, *18* (2), 423–429.
- (68) Johnstone, D. N.; Crout, P.; Nord, M.; Laulainen, J.; Høgås, S.; Opheim, E.; Martineau, B.; Bergh, T.; Francis, C.; Smeets, S.; Prestat, E.; Collins, S.; Hjorth, I.; Morzy, J.; Ånes, H. *Pyxem/Pyxem: Pyxem 0.10. 0.*; Zenodo, 2020.